Journal of Geophysical Research: Earth Surface

RESEARCH ARTICLE
10.1029/2018JF004779

Modeling Sediment Transport in Ice-Walled Subglacial Channels and Its Implications for Esker Formation and Proglacial Sediment Yields

Flavien Beaud[1,2], **Gwenn E. Flowers**[1], **and Jeremy G. Venditti**[3]

[1]Department of Earth Sciences, Simon Fraser University, Burnaby, British Columbia, Canada, [2]Now at Division of Geological and Planetary Sciences, California Institute of Technology, Pasadena, CA, USA, [3]Department of Geography, Simon Fraser University, Burnaby, British Columbia, Canada

Key Points:
- A framework is presented for sediment transport in subglacial channels over semialluvial beds
- Hysteresis in sediment and water flux is inherent to R-channels regardless of bed alluviation
- The formation of eskers is caused by a sediment bottleneck at the glacier terminus

Supporting Information:
- Supporting Information S1
- Figure S1
- Figure S2
- Figure S3
- Figure S4
- Figure S5
- Figure S6

Correspondence to:
F. Beaud,
fbeaud@caltech.edu

Citation:
Beaud, F., Flowers, G., & Venditti, J. G. (2018). Modeling sediment transport in ice-walled subglacial channels and its implications for esker formation and proglacial sediment yields. *Journal of Geophysical Research: Earth Surface*, *123*, 3206–3227. https://doi.org/10.1029/2018JF004779

Received 1 JUN 2018
Accepted 14 NOV 2018
Accepted article online 16 NOV 2018
Published online 6 DEC 2018

Abstract Sediment yields from glacierized basins are used to quantify erosion rates on seasonal to decadal timescales as well as conditions at the glacier bed, and eskers hold valuable information about past subglacial hydraulic conditions in their spatial organization, geometry, and sedimentary structures. Ultimately, eskers are a record of past glacio-fluvial sediment transport, but there is currently no physical model for this process. We develop a 1-D model of morphodynamics in semicircular bedrock-floored subglacial channels. We adapt a sediment conservation law developed for mixed alluvial-bedrock conditions to subglacial channels. Channel evolution is a function of melt opening by viscous heat dissipation from flowing water and creep closure of the overlying ice, to which we add the closure or enlargement due to sediment deposition or removal, respectively. We apply the model to an idealized land-terminating glacier and find that temporary sediment accumulation in the vicinity of the terminus, or the formation of an incipient esker, is inherent to the dynamics of the channelized water flow. The alluviation of the bed combined with the pressurized channel flow produces unexpected patterns of sediment evacuation: We show that the direction of hysteresis between sediment and water discharge is not necessarily linked to a supply- or transport-limited system, as has been hypothesized for proglacial sediment yields. We also find that the deposition of an incipient esker is a function of a compromise between water discharge and sediment supply, but perhaps more importantly, ice-surface slope and the temporal pattern of water delivery to the bed.

Plain Language Summary Glaciers and ice sheets are changing rapidly, impacting sea levels, landscapes, and ecosystems. These changes are tightly linked to the meltwater routing through glaciers' plumbing systems. If this plumbing is pressurized by water flowing into crevasses and moulin (which act like water wells), the ice base can move faster downstream, possibly leading to enhanced ice loss, or vice versa. As glaciers retreated at the end of the last glaciation, they left clues of their passage, including sediment casts of their plumbing system: eskers. Eskers are elongated ridges that snake across the landscape and can be hundreds of kilometers long. Although understanding their deposition can help us understand contemporary ice sheet plumbing systems, their origin has been puzzling for several decades. We build a numerical model tracking sediment as they move with the water under ice. Glaciers naturally produce a sediment bottleneck and tend to form such eskers, producing the first process-based model for their deposition. We identify ice geometry and temporal patterns of water input into the plumbing system as critical factors, when combined with sufficient sediment and water supplies. This model helps to reconcile contemporary glacier processes and sediment records, which is key to better understand glaciers' plumbing system.

1. Introduction

Observations of water-born sediment fluxes in proglacial areas are used to infer bedrock erosion rates and conditions at the ice-bed interface of contemporary glaciers and ice sheets (e.g., Gurnell et al., 1996; Hallet et al., 1996; Herman et al., 2015; Humphrey & Raymond, 1994; Koppes & Hallet, 2002, 2006; Koppes & Montgomery, 2009; Koppes et al., 2015; Loso et al., 2004; Mao et al., 2014; Orwin & Smart, 2004; Riihimaki et al., 2005; Sanders et al., 2013; Willis et al., 1996). On longer timescales, observations of subglacial landforms shaped by subglacial water flow provide insight into the basal conditions of former glaciers and ice sheets

(e.g., Bennett & Glasser, 2009; Brennand, 1994; Burke et al., 2015; Denton & Sugden, 2005; Dürst-Stucki et al., 2010; Dürst-Stucki et al., 2012; Jansen et al., 2014; Jørgensen & Sandersen, 2006; Kehew et al., 2012; Knight, 2003; Ó Cofaigh, 1996; Storrar et al., 2014; Stumm, 2010; van der Vegt et al., 2012). The interpretation of such observations relies on descriptive theories of sediment transport and bedrock erosion by subglacial water flow, yet a physical model combining such processes is still lacking. Unraveling proglacial sediment yields is thus key to understanding glacier dynamics, but also how glaciers impact their surrounding environments and ecosystems in a changing climate (e.g., Bhatia et al., 2013; Church & Ryder, 1972; Delaney et al., 2018; Overeem et al., 2017). In this study, we propose the first model of morphodynamics in semicircular bedrock-floored Röthlisberger channels (R-channels; Clarke, 2003; Röthlisberger, 1972) with transient sediment cover and contextualize our theoretical predictions to better interpret observations.

Most studies that quantify glacial erosion rates at timescales ranging from hours to several decades rely on measurements of proglacial sediment fluxes (e.g., Hallet et al., 1996; Herman et al., 2015; Koppes & Hallet, 2002, 2006; Koppes & Montgomery, 2009; Koppes et al., 2015; Loso et al., 2004; Riihimaki et al., 2005; Sanders et al., 2013). These exercises are contingent on the assumption that subglacial sediment storage is negligible and that subglacial water flow is the primary agent responsible for sediment evacuation. Proglacial sediment yields account for at least as much erosion as long-term erosion proxies (e.g., Koppes & Montgomery, 2009), with sediment entrainment by sliding ice often assumed to be much smaller (e.g., Alley et al., 1997; Cowton et al., 2012). Identifying the drivers of sediment evacuation is thus key to improving our understanding of glacial erosion.

On the timescales of glacial cycles, subglacial-water-born sediment transport shapes erosional and depositional landforms (e.g., tunnel valleys, inner gorges, and eskers) that offer a unique window into the basal conditions of past ice sheets (e.g., Bennett & Glasser, 2009; Brennand, 1994; Brennand, 2000; Burke et al., 2015; Burke et al., 2012; Clark & Walder, 1994; Denton & Sugden, 2005; Dürst-Stucki et al., 2010; Dürst-Stucki et al., 2012; Greenwood et al., 2016; Jansen et al., 2014; Jørgensen & Sandersen, 2006; Kehew et al., 2012; Knight, 2003; Livingstone & Clark, 2016; Ó Cofaigh, 1996; Storrar et al., 2014; Stumm, 2010; van der Vegt et al., 2012). Their origins are nonetheless the center of much debate (e.g., Beaud et al., 2016; Beaud et al., 2018; Brennand, 1994; Burke et al., 2015; Dürst-Stucki et al., 2010; Dürst-Stucki et al., 2012; Greenwood et al., 2016; Jansen et al., 2014; Kehew et al., 2012; Livingstone & Clark, 2016; Ó Cofaigh, 1996; Storrar et al., 2014; van der Vegt et al., 2012). Deciphering the formation of erosional features created by subglacial water flow is also key to planning safe repositories for nuclear waste in countries susceptible to large-scale glaciations in the next million years (e.g., Fischer et al., 2015). Subglacial flood flows are often invoked in order to explain the erosive power of water (Kehew et al., 2012; Wright, 1973; van der Vegt et al., 2012), the size of clasts found in eskers, or the large changes in flow regimes inferred from esker sediment (e.g., Brennand, 1994; Burke et al., 2012). Recent numerical modeling studies, however, suggest that pressurized seasonal meltwater flow produces sufficient shear stresses to transport boulder-size clasts and erode the bedrock (Beaud et al., 2016, 2018). The formation of eskers has been attributed to either the geology of the substrate (Clark & Walder, 1994), the availability of meltwater (e.g., Storrar et al., 2014), or the availability of sediment (e.g., Burke et al., 2015). While Burke et al. (2015) acknowledge the importance of a trade-off between sediment and water availability, they emphasize the importance of the quantity of sediment present. In general, it is well accepted that eskers form predominantly during stages of ice retreat over a rigid bed (e.g., crystalline bedrock), where a till veneer is present (e.g., Brennand, 2000; Clark & Walder, 1994).

Water flow mobilizes particles only if the shear stress it imparts on the bed exceeds a certain threshold (Shields, 1936). The value of this threshold depends on the characteristics of the channel floor and of the sediment mixture, for example, particle size, the size distribution of particles in the sediment mixture, the slope of the channel, or the roughness of the bed (e.g., Einstein, 1950; Garcia, 2000; García, 2008; Lamb, Dietrich, & Venditti, 2008; Meyer-Peter & Müller, 1948; Shields, 1936). Whether water flow tends to mobilize and remove or deposit sediment is a function of the ratio between the sediment transport capacity and sediment supply. If the supply exceeds the capacity, sediment is deposited; otherwise, it is removed. As a result, for an esker to be deposited, a negative divergence in sediment flux must occur, which can be induced by a change in sediment supply or transport capacity.

Studies of physical processes involved in sediment transport by subglacial water flow are rare, and they focus on distributed subglacial drainage systems (canals or macroporous sheets) assuming that the glacier bed is comprised of a thick layer of sediment (Carter et al., 2017; Creyts et al., 2013; Damsgaard et al., 2017;

Kyrke-Smith & Fowler, 2014; Fowler & Walder, 1993; Ng, 2000; Walder & Fowler, 1994). Canals are subglacial channels that can be carved both in ice and sediments and are associated with relatively low water discharge under ice sheets (e.g., Carter et al., 2017; Flowers, 2015; Walder & Fowler, 1994). Creyts et al. (2013) describe sediment fluxes and accretion by refreezing at the glacier bed in a macroporous water sheet and discuss how such sediment transport controls bed slopes close to the terminus of the glacier. Creyts et al. (2013) show the importance of water discharge fluctuations for sediment transport and discuss the implications for the evolution of bed slope.

Beaud et al. (2016) developed a model of bedrock erosion by subglacial water flow using a fluvial abrasion law (Lamb, Dietrich, & Sklar, 2008) in a supply-limited system. They showed that water flow-induced abrasion rates are negligibly small at the glacier scale, compared to expected ice flow-induced erosion rates. However, the localization of erosion in subglacial channels can lead to the excavation of significant bedrock channels (Beaud et al., 2016), especially on the timescale of a glacial cycle (Beaud et al., 2018). A few studies nevertheless identified a bottleneck in sediment transport in the vicinity of the glacier terminus, conditions prone to the deposition of eskers (Beaud et al., 2016; Drews et al., 2017), although sediment conservation was not implemented.

We develop a numerical model of sediment transport in R-channels, assuming that subglacial drainage occurs over a hard bed, till cover is relatively thin and patchy, and the surrounding distributed drainage system plays a negligible role in sediment transport. We combine equations describing water flow in a semicircular ice-walled bedrock-floored subglacial channel (Nye, 1976; Röthlisberger, 1972) with a law for sediment conservation suited for mixed bedrock-alluvial channels (e.g., Inoue et al., 2014; Nelson & Seminara, 2012; Zhang et al., 2015). After demonstrating the basic behavior of the model, we address the following questions: (1) What controls sediment delivery to proglacial streams? And (2) what controls sediment deposition and formation of incipient eskers? We then discuss the implications of the model results for the interpretation of proglacial sediment fluxes and the current theories on esker formation.

2. Methods

2.1. Governing Equations

We focus on sediment transport in straight ice-walled bedrock-floored semicircular R-channels with a transient sediment cover. In such R-channel the conservation of water is given by

$$-\gamma S_{\mathrm{ch}} \frac{\partial p_{\mathrm{ch}}}{\partial t} = \frac{\partial Q_{\mathrm{ch}}}{\partial x} + \frac{\Xi - \Pi}{L}\left(\frac{1}{\rho_{\mathrm{i}}} - \frac{1}{\rho_{\mathrm{w}}}\right) - v_{\mathrm{cc}} - \dot{b}_{\mathrm{ch}}, \tag{1}$$

where t and x are, respectively, time and position along the channel; γ is a fluid compressibility factor introduced for numerical purposes (Clarke, 2003); Q_{ch} is the water discharge in the channel; p_{ch} is the water pressure in the channel; Ξ is the dissipation of potential energy; Π is the change in sensible heat of the water; L is the latent heat of fusion; ρ_{i} and ρ_{w} are the densities of ice and water, respectively; v_{cc} is the creep closure rate of the channel; and $\dot{b}_{\mathrm{ch}}$ is a local water source term to emulate input from surrounding hydraulic systems (e.g., Flowers et al., 2004). The evolution of channel cross-sectional area S_{ch} with time is

$$\frac{\partial S_{\mathrm{ch}}}{\partial t} = v_{\mathrm{oc}} - v_{\mathrm{cc}} - v_{\mathrm{s}}, \tag{2}$$

where v_{s} is the sedimentation rate in the channel (e.g., Creyts et al., 2013; Ng, 2000; Walder & Fowler, 1994) defined as positive when sediment is being deposited and negative when it is removed. The opening rate of a channel by viscous heat dissipation is

$$v_{\mathrm{oc}} = \frac{\Xi - \Pi}{\rho_{\mathrm{i}} L}. \tag{3}$$

The creep closure rate is

$$v_{\mathrm{cc}} = \tilde{A} S_{\mathrm{ch}} |N_{\mathrm{ch}}|^{n-1} N_{\mathrm{ch}}, \tag{4}$$

where $\tilde{A}$ is a factor that includes Glen's flow-law coefficient and the shape of the channel, n is Glen's flow law exponent, and $N_{\mathrm{ch}} = p_{\mathrm{i}} - p_{\mathrm{ch}}$ is the effective pressure in the channel. The overburden ice pressure is $p_{\mathrm{i}} = \rho_{\mathrm{i}} g h_{\mathrm{i}}$, g is gravitational acceleration, and $h_{\mathrm{i}} = z_{\mathrm{i}} - z_{\mathrm{b}}$ is the ice thickness. The elevation of the bed, z_{b},

is the sum of the elevation of the bedrock, η_{br}, and the thickness of the sediment layer, η_a: $z_b = \eta_{br} + \eta_a$. For turbulent flow in a semicircular channel, the discharge is

$$Q_{ch} = -\left(\frac{8S_{ch}^3}{P_W \rho_w f_R}\right)^{1/2} \nabla\phi_{ch} |\nabla\phi_{ch}|^{-1/2}, \tag{5}$$

where $\phi_{ch} = \rho_w g z_b + p_{ch}$ is the hydraulic potential in the channel, P_W is the wetted perimeter, and the Darcy-Weisbach roughness is expressed as $f_R = 8g\langle n' \rangle^2 / R_H^{1/3}$, with $\langle n' \rangle$ the Manning roughness averaged over the channel perimeter. The hydraulic radius of the channel is

$$R_H = \frac{S_{ch}}{P_i + P_b}, \tag{6}$$

where $P_W = P_i + P_b$, $P_i = \pi\sqrt{\frac{2S_{ch}}{\pi}}$, and $P_b = 2\sqrt{\frac{2S_{ch}}{\pi}}$ are, respectively, the wetted perimeters of the whole channel, the ice walls, and the bed in a semicircular channel. The dissipation of potential energy is expressed as

$$\Xi = \left| Q_{ch} \frac{\partial \phi_{ch}}{\partial x} \right|, \tag{7}$$

and the change in sensible heat of the water is

$$\Pi = -c_t c_w \rho_w Q_{ch} \frac{\partial p_{ch}}{\partial x}, \tag{8}$$

where c_t is the pressure-melting coefficient and c_w is the heat capacity of water.

Morphodynamic modeling of mixed bedrock-alluvial channels has seldom been treated in the literature (cf. Inoue et al., 2014; Nelson & Seminara, 2012; Zhang et al., 2015). The general form of Exner's equation for alluvial rivers is

$$(1 - \lambda)\frac{\partial \eta_a}{\partial t} + \frac{\partial q_t}{\partial x} = 0, \tag{9}$$

where λ is the porosity of the sediment layer and q_t is the volumetric sediment flux per unit width. In channels with a patchy alluvial cover (i.e., mixed bedrock-alluvial channels) the thickness of sediment at rest can be zero, though sediment is being transported above the level of the bedrock. Exner's equation fails to capture such behavior; thus, a term must be added to account for the volume of sediment being transported. The sediment flux is smaller than the transport capacity and must be calculated as a function of the volume of available sediment. Several different formulations have been proposed to treat mixed bedrock-alluvial channels (Inoue et al., 2014; Nelson & Seminara, 2012; Zhang et al., 2015); we build on that of Inoue et al. (2014) where the volume of sediment in transport, V_b, per unit channel width and grid cell length is

$$\frac{\partial V_b}{\partial t} + (1 - \lambda)F_c \frac{\partial \eta_a}{\partial t} + \frac{\partial q_t}{\partial x} = 0, \tag{10}$$

where F_c is the fraction of the macrotopography of the bed covered by sediment. Sediment can be deposited in topographic lows while topographic highs remain exposed, or the bed can be fully covered, and $F_c = 1$. In Inoue et al. (2014), F_c is related to the macroroughness of the bed; we omit this level of complexity in the current study. Inoue et al. (2014) define the volumetric sediment flux per unit width as

$$q_t = \begin{cases} \frac{V_b}{V_{tc}} q_{tc}, & 0 \le \frac{V_b}{V_{tc}} < 1 \\ q_{tc}, & \frac{V_b}{V_{tc}} \ge 1 \end{cases}, \tag{11}$$

where q_{tc} is the volumetric transport capacity per unit channel width, here expressed as (Fernandez-Luque & van Beek, 1976)

$$q_{tc} = 5.7\left(rgD^3\right)^{1/2}\left(\tau^* - \tau_c^*\right)^{3/2}, \tag{12}$$

where $r = \rho_s/\rho_w - 1$ is the buoyant density of a particle of diameter D, ρ_s is the particle density, $\tau^* = \tau_b / \left((\rho_s - \rho_w)gD\right)$ is the Shields stress, and τ_c^* its critical value. The shear stress on the channel bed and walls can be expressed as

$$\tau_{tot} = \frac{1}{8} f_R \rho_w v |v|, \tag{13}$$

Table 1
Summary of Model Constants and Parameters

Parameter	Description	Value
$\tilde{A}$	Flow-law coefficient for channels	5×10^{-25} Pa^{-n} s^{-1}[a]
c_t	Pressure melting coefficient	7.5×10^{-8} K Pa^{-1}
c_w	Heat capacity of water	4.22×10^3 J kg^{-1}K^{-1}
D	Particle diameter	0.06 m
dx	Cell size	100 m
dt	Output time step	3,600 s
g	Gravitational acceleration	9.8m s^{-2}
L	Latent heat of fusion	3.34×10^5 J kg^{-1}
n	Flow-law exponent	3
n'_b	Manning roughness for bed	0.05[b]
n'_i	Manning roughness for ice	0.01[b]
$\langle n' \rangle$	Manning roughness averaged	0.0321[c]
X_L	Glacier length	30 km
γ	Numerical compressibility parameter	10^{-9} Pa^{-1}
λ	Porosity of sediment	0.35
ρ_i	Ice density	910 kg m^{-3}
ρ_s	Sediment particle density	2,650 kg m^{-3}
ρ_w	Water density	1,000 kg m^{-3}
τ_c^*	Critical shear stress	0.03

[a]See Werder et al. (2013). [b]Chosen to obtain a reasonable $\langle n' \rangle$; see also the supplement of Beaud et al. (2016). [c]See Clarke (2003) and also Table 1 in Gulley et al. (2014) for a review of values used in numerical models and measured in the field.

where $v = Q_{ch}/S_{ch}$ is the water velocity, and the averaged friction coefficient in a semicircular channel (Clarke, 2003)

$$f_R = \frac{f_i P_i + f_b P_b}{P_i + P_b} = \frac{f_i P_i + f_b P_b}{P_W}. \tag{14}$$

The friction coefficients for the ice wall and bed are

$$f_i = \frac{8g{n_i}'^2}{R_H^{1/3}} \text{ and } f_b = \frac{8g{n_b}'^2}{R_H^{1/3}}, \tag{15}$$

respectively, with the Manning roughness coefficients: n_i' for the ice and n_b' for the bed. The shear stress on the bed is

$$\tau_b = \frac{1}{8} f_b \rho_w v |v|. \tag{16}$$

The saturation volume of sediment per unit area (Inoue et al., 2014; i.e., the threshold above which the volume of sediment in transport is sufficiently high that the bed alluviates) is

$$V_{tc} = \frac{q_{tc}}{u_s}, \tag{17}$$

and the sediment saltation velocity u_s is defined according to Sklar and Dietrich (2004):

$$u_s = 1.56 \left(\frac{\tau^*}{\tau_c^*} - 1 \right)^{0.56} \sqrt{rgD}. \tag{18}$$

Note that with this empirical expression (equation (18)) u_s must be capped at the water flow velocity (Beaud et al., 2016; Lamb, Dietrich, & Sklar, 2008). To accommodate spatio-temporal changes in channel width and

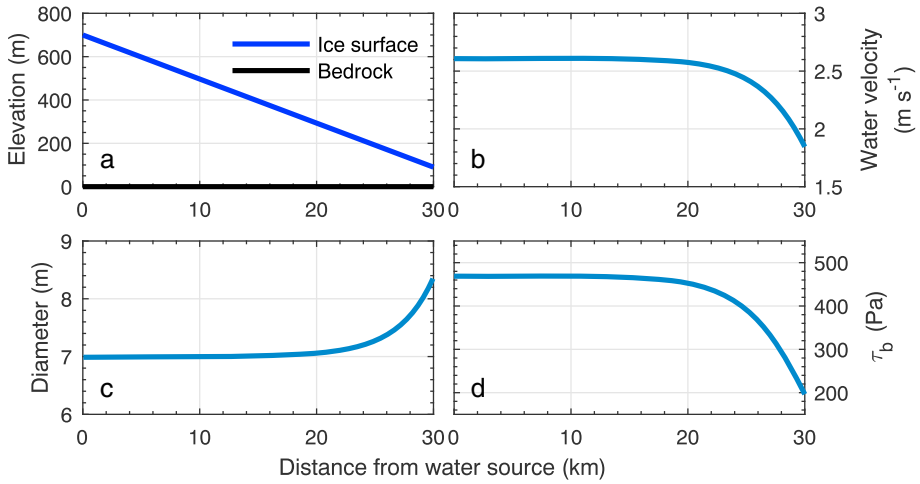

Figure 1. Hydraulic quantities computed when steady state has been reached with a constant discharge $Q_{ch}(x = 0) = 50\,m^3\,s^{-1}$ in the absence of sediment. (a) Ice surface z_i and bedrock elevation η_{br}; (b) water velocity $v = Q_{ch}/S_{ch}$; (c) R-channel diameter W_{ch}; and (d) shear stress exerted on the bed τ_b (equation (16)). Note that the quantities plotted appear constant between kilometers 0 and 18 in panels (b)–(d), although they are not; changes are too small to be easily visible.

bed shear stresses of an order of magnitude during the simulations, we use the total volume of sediment in a channel reach per unit length V_s, instead of the sediment thickness η_a, which is a width averaged quantity, such that

$$V_s = \left(V_b + (1-\lambda)F_c\eta_a\right) W_{ch}, \tag{19}$$

where W_{ch} is the width of the R-channel. Since we omit the macroroughness of the bed, we replace the fraction covered F_c by the ratio between the volume of sediment available and that available to be transported:

$$r_V = \begin{cases} \frac{V_s}{V_{tc}W_{ch}}, & 0 \le \frac{V_s}{V_{tc}W_{ch}} < 1 \\ 1, & \frac{V_s}{V_{tc}W_{ch}} \ge 1 \end{cases}, \tag{20}$$

and thus, the total sediment flux in a given reach is

$$q_{tt} = q_{tc}r_V W_{ch}. \tag{21}$$

We also define the sediment transport capacity in a reach as

$$q_{ttc} = q_{tc}W_{ch}. \tag{22}$$

The conservation of sediment becomes

$$\frac{\partial V_s}{\partial t} + \frac{\partial q_{tt}}{\partial x} - \frac{q_{ls}}{dx} = 0, \tag{23}$$

where q_{ls} is a local sediment input term from the surrounding environment. The rate of change of channel cross-sectional area due to sediment deposition or entrainment (equation (2)) is found by calculating the change in equivalent sediment cross-sectional area resulting from the change in sediment volume:

$$v_s = \frac{\partial V_s}{\partial t}\frac{1}{(1-\lambda)}. \tag{24}$$

We solve the system of equations comprising the conservation of water (equation (1)), the evolution of the channel cross-sectional area (equation (2)), and the evolution of sediment volume (equation (23)) for p_{ch}, S_{ch}, and V_s with the Matlab® `ode15s` solver and the parameters summarized in Table 1.

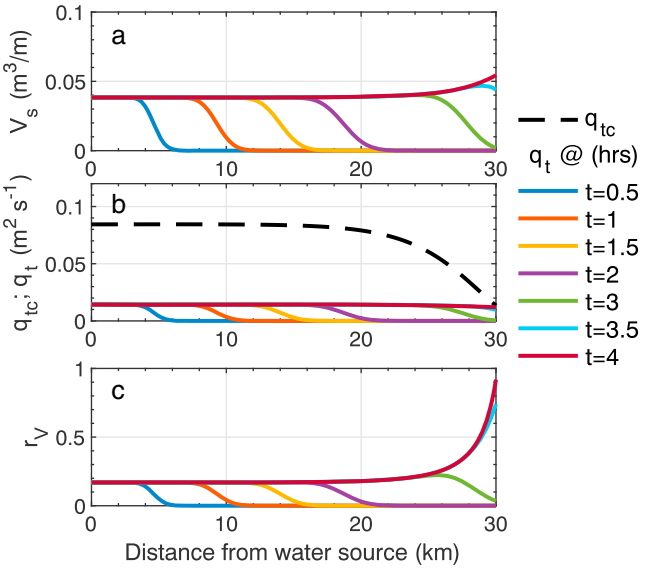

Figure 2. Evolution of sediment transport in an decoupled simulation with steady-state hydrology; that is, S_{ch} and p_{ch} are in steady state (section 3.2.1; Figure 1). (a) Volume of sediment per unit length V_s. (b) Volumetric transport capacity q_{tc} (dashed) and sediment flux q_t (solid lines) per unit width. (c) Ratio between volume of sediment in a reach and volume transported at capacity r_V.

2.2. Initial and Boundary Conditions

We prescribe the water discharge at the upstream end of the domain ($Q_{ch}(x = 0)$), and we set the water pressure at the downstream end to be atmospheric ($p_{ch}(x = X_L) = 1{,}000$ Pa). As there is no water input along the channel path and the contribution of ice-wall melt is marginal, input and outlet water discharge are virtually the same. We prescribe the sediment input at the upstream end of the domain ($q_{ls}(x = 0)$) or apply a no-flux boundary condition ($\frac{\partial q_{tt}}{\partial x}(x = 0) = 0$). The transport capacity is largely influenced by the shape of the hydrograph, and sediment discharges at the terminus change by over 1 order of magnitude throughout the simulations presented. If too much sediment is fed to the system, the numerical model becomes unstable because the channel closes with sediment faster than it can open due to the water flow. On the other hand, if the sediment supply is easily evacuated, no sediment deposition occurs, and the system behaves as a traditional R-channel. We thus have to adjust sediment input accordingly, and the choice of specific values is justified in each subsection. We assume a constant gradient in $\partial S_{ch}/\partial t$ at the terminus. We spin up every simulation for a sufficient time that the results are independent of initial conditions. The spin-ups are described individually for each simulation.

3. Simulation Setup and Results

3.1. Model Setup

The model domain comprises a single R-channel fed by a moulin, and we neglect the interactions between different types of drainage systems (see Flowers, 2015, for a review). Our reference glacier geometry is defined by a constant ice surface slope and a flat bed (Figure 1a). We chose this geometry because (1) it is a reasonable profile for the terminus of a retreating glacier and (2) it produces a constant ice overburden pressure gradient that helps to disentangle the interactions between the sediment transport and ice-walled channel. All the simulations feature a constant sediment supply ($q_{ls}(x = 0)$) and a constant sediment size ($D = 0.06$ m), which we assume is a representative grain size for the subglacial sediment (e.g., Riihimaki et al., 2005). We assume that the sediment volume, V_s, is distributed uniformly across the channel bed. We first present simulations where sediment transport and water flow are decoupled (V_s calculated, but $v_s = 0$ in equation (2), so bed alluviation can occur but does not affect channel size) and the water input is constant. We then present results with the coupled model and test the role of temporal fluctuations in water input. Additional testing of the model sediment conservation (supporting information S1 and Figure S1), the influence of time step on the results (supporting information S1 and Figure S2), the influence of grid size on the solution (supporting information S2 and Figure S3), and the removal of an initial layer of sediment (Figure S4) can be found in the supplement.

Table 2
Simulations With a Constant Water and Sediment Input

Simulation	$q_{ls}(x = 0)\,(m^3\,s^{-1})$	$V_s(x = X_L)\,(m^2)$	$S_{ch}(x = X_L)\,(m^2)$	$q_{ttc}\,(x = X_L)\,(m^3\,s^{-1})$
R1	0.200	0.23	27.41	0.200
R2	0.205	0.41	27.23	0.205
R3	0.210	0.60	27.05	0.210
R4	0.215	0.11–2.18	26.89 – 26.9	0.2146–0.2156

Note. See Figure 3 and section 3.2.2.

3.2. Simulations With Constant Water Input

3.2.1. Decoupled Simulations

To test the effect of a simple shear-stress field and channel-size profile on sediment transport, we perform a simulation with constant water ($Q_{ch}(x = 0) = 50\,m^3\,s^{-1}$) and sediment input ($q_{ls}(x = 0) = 0.1\,m^3\,s^{-1}$), both prescribed at the upstream boundary. The sediment is only added once the hydrologic system (p_{ch} and S_{ch}) has reached a steady state, which are the conditions shown in Figure 1. The sediment input was chosen to be less than the transport capacity at the terminus to show the transport of sediment without sediment accumulation. A similar test, but using an initial layer of sediment rather than an upstream sediment flux, is described in the supplement (section S1 and Figure S1).

With a constant ice-surface slope, a flat bed and a constant discharge (Figures 1a and 1b), the water velocity decreases monotonically toward the terminus; this decline is enhanced over the last 10 km of the profile (Figure 1b) as a result of the increase in channel size (Figure 1c). The creep closure rate of the R-channel decreases as the ice thins, enlarging the channel. The shear stress pattern follows that of the water velocity, suggesting a bottleneck close to the glacier terminus (Figure 1d). In this scenario, it only takes about 4 hr for an advancing front of sediment to travel through the 30-km domain and for the sediment volume (V_s) to reach a steady state (Figure 2a). The conditions are always supply limited, and the sediment flux remains a fraction of the transport capacity (Figures 2b and 2c). The slight increase in sediment volume over the last 5 km of the profile is the result of the drop in water-flow velocity and therefore sediment velocity (Figure 1b).

3.2.2. Coupled Simulations With Constant Water and Sediment Input

In order to test the effect of the coupling between sediment transport and water flow, we perform a series of simulations with different rates of sediment input ($q_{ls}(x = 0)$; Table 2). The prescribed rates of sediment input are chosen to exceed the transport capacity at the terminus for a decoupled steady-state simulation. The value of $q_{ls}(x = 0)$ is increased until the system fails to reach a steady state (Table 2). In this series of simulations, the sediment and water input are constant from the beginning, in contrast to the previous simulations where the sediment input was only introduced once the hydrology (i.e., S_{ch} and p_{ch}) had reached a steady state.

All simulations (R1 – R4; Table 2) start with a damped oscillation in sediment volume at the terminus and reach a steady state after ~150 days, except R4, which exhibits a 22-day periodic oscillation (Figure 3a). The damped oscillation is caused by the difference in response time between the sediment cover (minutes to hours) and the channel walls (days to weeks). As the channel forms, it enlarges until the transport capacity drops sufficiently for sediment accumulation to occur (Figure S5). The channel then fills up with sediment, the hydraulic pressure gradient steepens, and the sediment is rapidly removed, thereby enlarging the channel (Figure 3b). As creep is not sufficient to close the channel and maintain hydraulic pressure gradients (Figure S5), the transport capacity again drops, leading to sediment deposition. In simulations R1 – R3 the sediment supply is such that a sediment wedge reaches equilibrium (Figure 3c). The cross-sectional area of the channel is reduced (Figure 3d), and the hydraulic potential gradient increases (Figure 3e) such that the transport capacity at the terminus reaches the value of the sediment supply imposed (Figure 3e). It is interesting to note that the difference in channel cross-sectional area between simulations is smaller (~0.36 m^2 smaller in R3 than R1; Figure 3d) than the difference between the area occupied by sediment (~0.57 m^2 once corrected for sediment porosity; Figure 3c). The increase in water velocity should lead to enhanced channel melt and thus a larger channel at the terminus for R3 than R1. The adverse slope of the bed created by the sediment wedge is sufficient to dissipate energy that is no longer available for melting. The increase in the sensible heat (Π; equation (8)) is larger than that of the dissipation of potential energy (Ξ; equation (7)); thus, the rate of channel opening ($v_{oc} \propto \Xi - \Pi$; equation (3)) decreases.

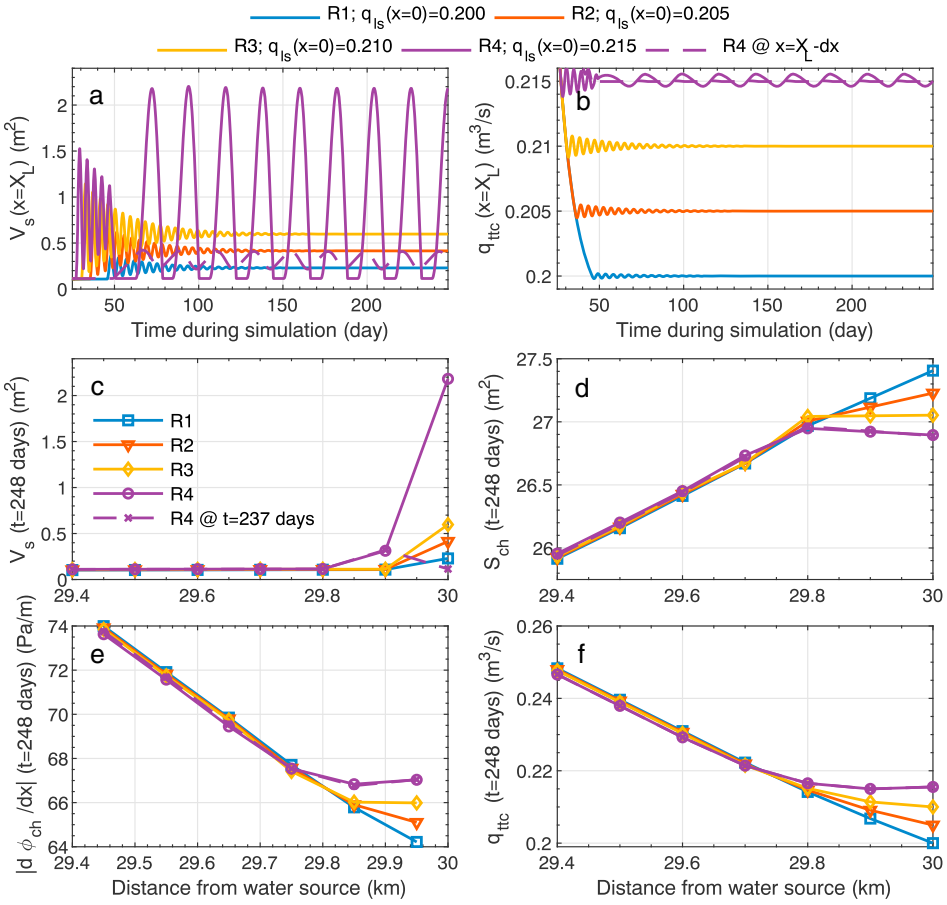

Figure 3. Temporal and spatial variations in selected variables showing the interaction between sediment bottleneck and hydrology. Temporal evolution of (a) sediment volume, V_s, and (b) transport capacity at the terminus ($q_{ttc}(x = X_L)$. Spatial changes within the last 0.6 km of the profile at the end of each simulation of (c) sediment volume per unit length V_s, (d) cross-sectional area of the channel S_{ch}, (e) magnitude of the hydraulic potential gradient $|\partial\phi_{ch}/\partial x|$, and (f) sediment transport capacity q_{ttc}. Note that R4 is shown at a local maximum and minimum because it does reach a steady state.

For simulation R4, the sediment wedge is large enough that the transport capacity at 30 km can be larger than that at 29.9 km (Figures 3b and 3f), instead of monotonically decreasing as in R1 – R3. The location of the bottleneck oscillates between 29.9 and 30 km. Sediment accumulates faster at 30 km such that the channel constriction by sediment is sufficient to raise the transport capacity above that at 29.9 km. Sediment is then evacuated at 29.9 km faster than it accumulates, and the volume at 30 km continues to increase. As the transport capacity at 30 km is able to remove the sediment present, the channel size increases again, and transport capacity decreases. This allows for sediment to start accumulating at 29.9 km again.

In this set of simulations, we do not show the results with a decoupled model. The channel evolution for a sediment supply smaller than the outlet transport capacity is virtually the same as shown in Figure 2. On the other hand, if the sediment supply exceeds the transport capacity at any location, sediment wile gradually be deposited because the feedback between sediment deposition and transport capacity is lacking.

3.3. Simulations With Variable Water Input

3.3.1. Water Input Frequency

The timescale for channel cross-sectional area adjustment is on the order of a few hours for sediment transport, but on the order of several days for viscous heat dissipation and creep combined. The coupled system response (Figure 3) is therefore nontrivial even under constant forcing. To identify how these processes interact under varying water input despite such different response times, we perform simulations with sinusoidal fluctuations in water discharge of identical amplitude, but with four different arbitrary periods: 1 day, 6 days, 1 month, and 3 months. Sediment input remains constant and unchanged for these simulations and was

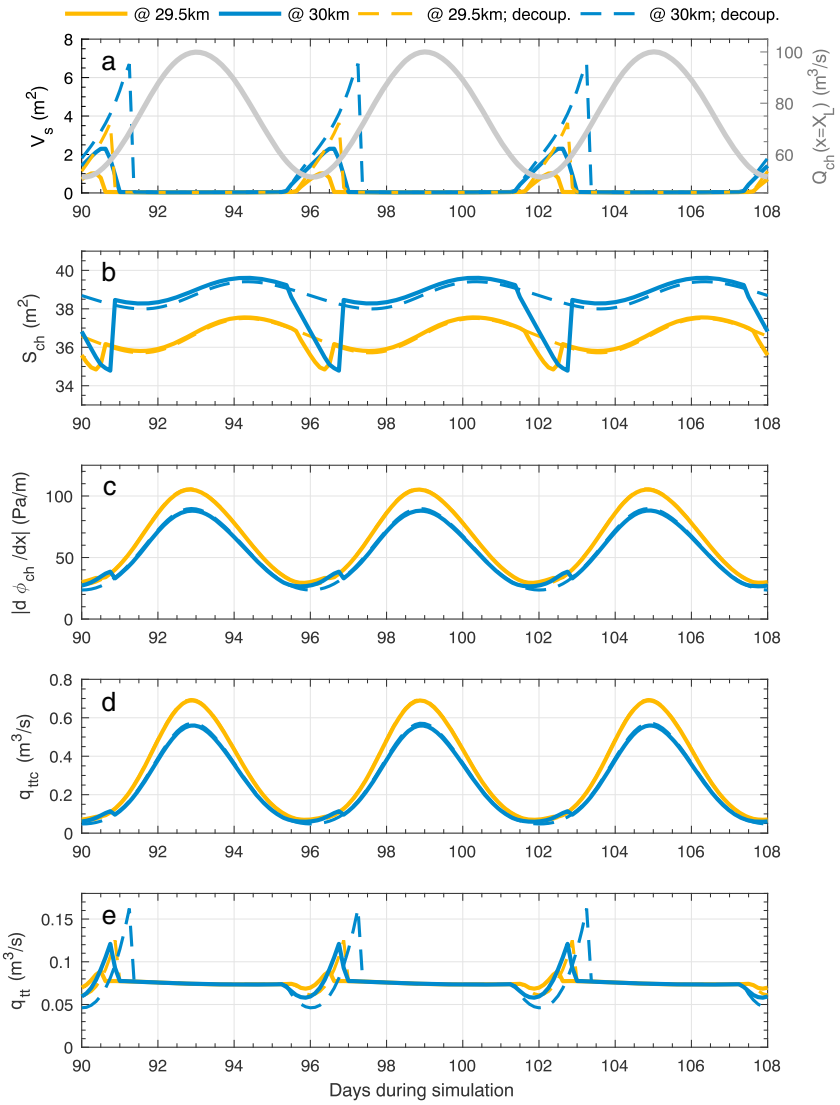

Figure 4. Temporal evolution of key quantities near the terminus for a water input forcing period of 6 days. (a) Volume of sediment per unit length and outlet water discharge (gray). (b) Channel cross-sectional area. (c) Magnitude of the hydraulic potential gradient. (d) Transport capacity. (e) Volumetric discharge of sediment. The dashed lines represent a simulation where sediment transport and channel evolution are decoupled. Quantities are shown at 29.5 and 30 km from the water source for three forcing cycles after a 90-day spin-up.

chosen so that the solution remained stable across the range of conditions tested, while sediment accumulation is possible in most. We perform simulations both with and without coupling sediment transport to channel cross-section evolution. These simulations are spun up for 90 days to allow for the system to reach a dynamic steady state, that is, a state where values oscillate between a minimum and maximum around a central value. The bottleneck occurs in the vicinity of the terminus; we thus describe the results only in this area. The rest of the profile remains supply limited; conditions are examined in Beaud et al. (2016).

When we prescribe a 6-day oscillation in water input (Figure 4), a temporary sediment accumulation starts half a day before the water discharge minimum occurs and lasts for 1.5 to 2 days. The resulting sediment bottleneck is strongest and lasts the longest at the terminus, decreases in size up-glacier (Figure 4a), and is larger when sediment and water flow are not coupled. As sediment fills the channel (Figure 4b), hydraulic potential gradients (Figure 4c) and transport capacities (Figure 4d) are larger than in a channel without sediment (dashed lines). At relatively high discharges, the system is supply limited; thus, the sediment discharge is virtually constant (Figure 4e). At low discharges, however, the bed is alluviated, and the system transport is limited ($r_V = 1$ and $q_{tt} = q_{ttc}$). The rate at which sediment accumulates at the beginning of a cycle depends strongly

Table 3
Summary of Simulations With Different Forcing Periods Shown in Figures 4 and 5

Water forcing period	Max $\left(\frac{V_s(x=X_L)}{1-\lambda}\right)$ (m^2)	Max $\left(\frac{V_s(x=29.5\,km)}{1-\lambda}\right)$ (m^2)	Consecutive hours with $r_v = 1$ at 30 km
1 day	0.69	0.09	4
6 days	3.53	1.57	37
1 month	6.57	0.10	165
3 months	0.08	0.07	0

Note. For these simulations $q_{ls}(x = 0) = 0.075\,(m^3/s)$ and the values reported in the table are only for the coupled simulations.

on how stark the bottleneck is. Sediment is rapidly removed from the bed at the end of each cycle because the transport capacity increases quickly. For example, under a constant hydraulic forcing, a sediment layer of half a meter could be stripped of a 4-km section of the bed in 4 hr (Figure S4)

The range of forcing frequencies tested leads to behaviors where changes in cross section are dominated by either sediment transport (1-day) or evolution of the ice walls (3-month; Figure 5). When a 1-day frequency is imposed, sediment accumulation occurs for 4 hr (Table 3), although it is focused within 500 m of the terminus and the amount of sediment occupying the channel remains modest (~0.4–0.7 m^2, equivalent to a sediment layer one-grain thick). The changes in discharge are sufficiently rapid that the channel walls remain virtually steady, as shown by the decoupled model (Figure 5b; dotted line). The most sediment accumulation occurs when changes in channel size due to ice-wall evolution and sediment transport are comparable in size (Figures 5c–5f; 6-day and 1-month frequencies). The sediment accumulation at 30 km is largest for the 1-month frequency, but its extent is limited to the last 500 m of the glacier. The ice is sufficiently thick at 29.5 km that creep closure can adjust in concert with discharge. The creep closure scales with the effective pressure raised to the power of three (equation (4)), making the bottleneck in sediment transport particularly efficient. In contrast, the 6-day forcing produces a shallower sediment wedge at the terminus, though it extends almost 1-km upglacier from the terminus, as thicker ice responds faster to the higher forcing frequency. Finally, applying a 3-month forcing frequency yields no sediment accumulation (Table 3), although fluctuations in sediment volume occur due to spatio-temporal changes in particle velocity. Over the 3-month period, channel walls can adjust in conjunction with water discharge, and the transport capacity remains sufficiently large to prevent sediment accumulation. As a result the changes in channel evolution between the coupled and decoupled simulations are imperceptible. It is also interesting to note that the fluctuations displayed in Figure 5e for the 1-month period have a similar origin as those observed for R4 in Figure 3. Local minima in sediment discharge temporarily occur upstream from the terminus over the sediment layer, creating successive sediment pulses.

3.3.2. Seasonal Water Input

Having established the different responses of the system to a range of water forcing frequencies, we construct a synthetic discharge time series intended to represent a melt season (Figure 6a). We explore how the system responds to a combination of water forcing frequencies and how the forcing influences sediment delivery to the proglacial area. The sediment input is kept constant ($q_{ls}(x = 0) = 0.030\,m^3\,s^{-1}$) at a value chosen to produce sediment accumulation and conservative values of sediment concentration at the outlet compared to published observations (see section 4.1). The simulation is run for two melt seasons, with the first serving as a spin-up.

The sediment volume per unit length (V_s) remains lower than 0.03 m^2 during the first part of the melt season (up to day 84), but significant sediment accumulation occurs in the second part of the melt season (after day 84; Figure 6b). This change in behavior is concomitant with a significant drop in water discharge because creep closure is too slow to sustain hydraulic pressure gradients (Figure 6c). The resulting sediment bottleneck leads to episodes of bed alluviation spanning one to several days and extending several hundred meters upstream from the terminus (Figure 6d). In the second part of the melt season, most of the channel bed remains supply limited except the last several hundred meters at the downstream end, where alluviation will control the sediment fluxes exiting the glacier.

3.4. Hysteresis Between Sediment and Water Discharge

The typical method to quantify seasonal proglacial sediment yields in the field is to measure water discharge and suspended sediment concentration, since direct measurements of sediment fluxes are extremely

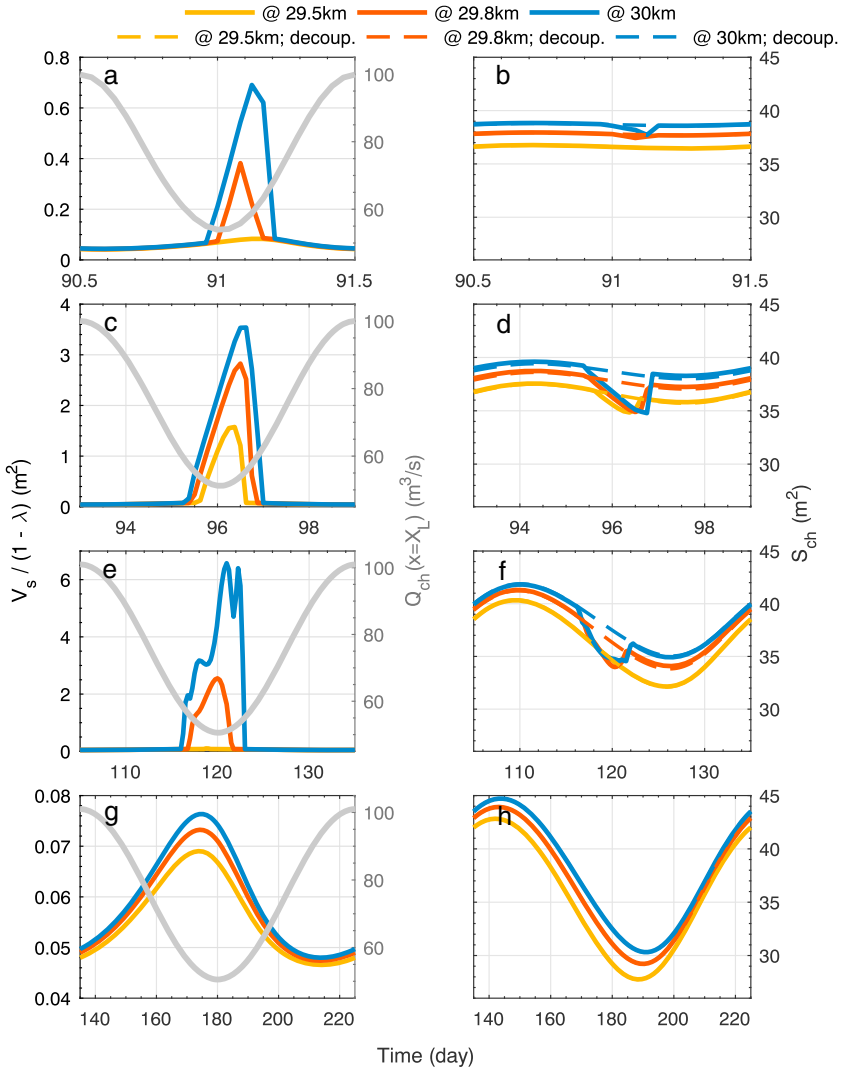

Figure 5. Comparison of the temporal evolution of channel cross-sectional area occupied by sediment ($V_s/(1-\lambda)$) and water discharge (Q_{ch}; a, c, e, and g in the left column) and channel cross-sectional area (b, d, f, and h in the right column) near the terminus for four different forcing frequencies: (a, b) 1 day; (c, d) 6 days; (e, f) 1 month; and (g, h) 3 months (Table 3). The 6-day forcing is shown in detail in Figure 4. Full lines represent results from the simulation where sediment and water flow are coupled and dashed lines where they are decoupled. For discharge and channel cross-sectional area the *y*-axes have the same scale in the figure while the *x*- and *y*-axes change for time and sediment volume such that only one oscillation is represented for each frequency.

challenging (e.g., Gurnell et al., 1996; Mao et al., 2014; Orwin & Smart, 2004; Riihimaki et al., 2005; Willis et al., 1996) and bedload flux quantification remains exceptional (e.g., Riihimaki et al., 2005; Mao et al., 2014). Hysteresis between sediment fluxes and water discharge is also widely used to interpret how sediment fluxes relate to subglacial sediment availability. A common assumption is that clockwise hysteresis, defined here as sediment transport peaking before water discharge, indicates that the channel is sediment starved (e.g., Mao et al., 2014; Riihimaki et al., 2005; Willis et al., 1996).

With the prescribed constant sediment input, sediment discharge is virtually constant over the first part of the melt season but exhibits strong daily fluctuations in the second part when alluviation occurs (Figure 7a). The daily sediment discharge fluctuations are effective up to several hundred meters upstream from the terminus. If we consider the whole season, water discharge peaks on day 45 while sediment discharge peaks on day 107 (Figures 6 and 7), exhibiting a counter-clockwise hysteresis that may be interpreted as implying transport-limited conditions. This is, however, not the case, as no sediment remains at the end of the simulation (Figure 7b).

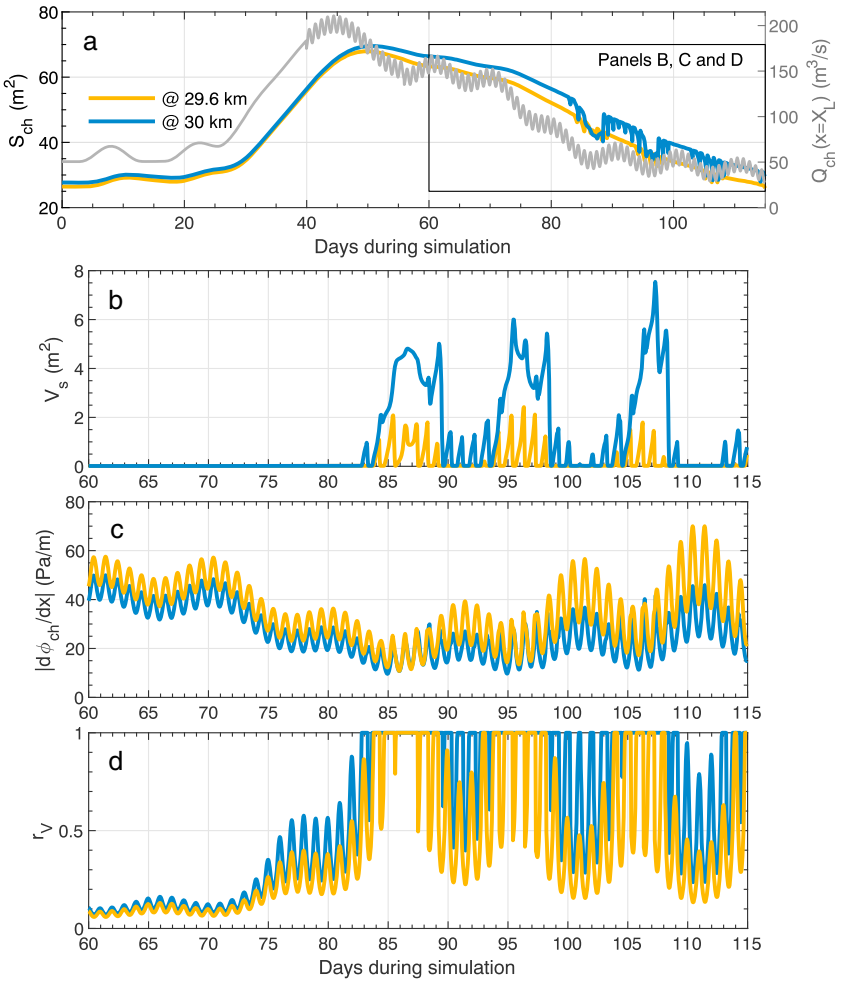

Figure 6. Temporal evolution at the terminus (30 km) and 400-m up-glacier (29.6 km) of (a) channel cross-sectional area and water discharge (gray); the panel represents the time window selected for the subsequent plots. (b) Sediment volume per unit length. (c) Magnitude of the hydraulic potential gradient. (d) Volume ratio r_V. An alluvial cover is present when $r_v = 1$. Quantities are shown for simulations with a synthetic melt season and a constant sediment input $q_{ls}(x = 0) = 0.03\ m^3/s$ (Table 4). Note that for (b)–(d) only a subset of the synthetic melt season (day 60 to day 115) is shown.

In the second part of the melt season, peaks in sediment discharge (days 88, 97–98, and 104–106) occur on the rising limb of multiday discharge fluctuations (days 87–91, 96–101, and 106–111), thus showing a clockwise hysteresis. Expectations are met here: hysteresis coincides with the transition from a transport- to supply-limited bed, and the bed is depleted of sediment when discharge peaks. Both clockwise and counter-clockwise events are present in the daily hysteresis (Figure 7b). Counter-clockwise events coincide with an alluviated bed, although clockwise events occur regardless of the alluviation. Neither supply- nor transport-limited conditions at the bed of the channel are uniquely associated with the direction of hysteresis between sediment and water discharge. Beaud et al. (2016) showed that the lag between peak shear stress and peak discharge depends on whether the channel is enlarging or contracting on timescales longer than several days. In a growing channel, water velocities peak before discharge, resulting in a clockwise hysteresis between sediment transport and discharge; the opposite is true in a closing channel. This is also the reason that counterclockwise events are observed primarily at the terminus, and their number decreases with distance up-glacier (Figure 7B). Ice thickness increases with distance from the terminus, increasing the efficiency of creep closure. The thicker the ice, the more rare it is for the channel to display multi-day periods with a closing trend, because the response time of the channel is relatively short.

Table 4
Summary of Simulations to Test Sediment Accumulation in Figures 6–9

Simulation	Ice geometry	Q_{ch}	$q_{ls}(x=0)$ (m^3s^{-1})	max(η_a) (m)	max η_a extent (km)	Figure
S1	$h_i(x) = 700 - \frac{700-90}{3\times10^5}x$	Reference	0.03	1.33	1.2	6–8, and 9a
S2	$h_i(x) = 610 \times (3\times10^5 - x)^{1/1.3} + 90$	Reference	0.03	2.75	0.3	9b
S3	$h_i(x) = 800 - \frac{800-90}{3\times10^5}x$	Reference	0.03	1.28	1.0	9c
S4	$h_i(x) = 600 - \frac{600-90}{3\times10^5}x$	Reference	0.03	1.10	1.6	9d
S5	$h_i(x) = 700 - \frac{700-90}{3\times10^5}x$	$Q_{ch,\,ref} \times 0.8$	0.03	1.18	1.4	9e
S6	$h_i(x) = 700 - \frac{700-90}{3\times10^5}x$	$Q_{ch,\,ref} \times 1.2$	0.03	1.00	1.1	9f
S7	$h_i(x) = 700 - \frac{700-90}{3\times10^5}x$	Reference	0.025	0.86	1.1	9g
S8	$h_i(x) = 700 - \frac{700-90}{3\times10^5}x$	Reference	0.035	1.27	1.4	6h

3.5. Sediment Accumulation in the Vicinity of the Terminus

The geography of esker ridges and their sedimentary deposits have been extensively described, revealing some intriguing characteristics. Some esker ridges span several hundred kilometers across the Canadian Shield (e.g., Storrar et al., 2014) or have sediment sizes ranging from sand to boulders (e.g., Brennand, 1994). Nevertheless, a unifying process-based theory to explain their deposition is still lacking. Burke et al. (2015) infer that a trade-off between sediment and water supply is required and find that the longitudinal sedimentary deposits of eskers show three main types of accretionary structure: (1) up-glacier, (2) vertical, and (3) down-glacier.

To investigate esker formation, we convert the sediment volume, V_s, into a sediment thickness $\eta_a = V_s/\left(W_{ch}(1-\lambda)\right)$ and show its evolution in time, that is, the resulting sedimentary deposits (Figure 8). From equation (19) it follows strictly that $\eta_a = (V_s - V_b W_{ch})/((1-\lambda)W_{ch})$; however, when a significant sediment layer is present, V_b is negligible.

Since sediment deposition occurs in the later melt season (see Figure 6), we focus on days 93–97 (Figure 8a). The formation of a sediment deposit requires that spatial sediment distribution changes in time. To show how the model results could be paralleled to field observations, we focus on snapshots separated by only a few

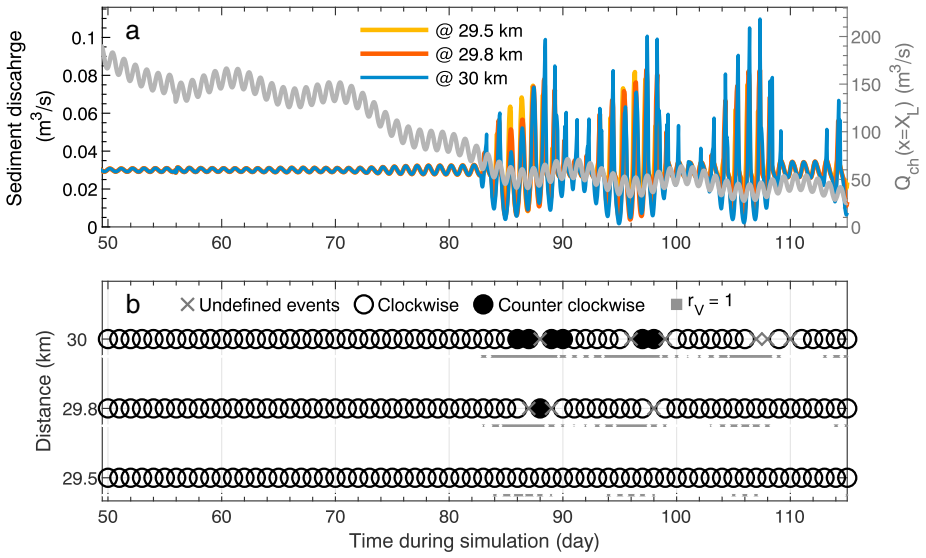

Figure 7. Temporal evolution near the terminus of (a) sediment and water discharge (gray). (b) Daily hysteresis between sediment (q_{tt}) and water discharge (Q_{ch}). The gray square show when the bed is alluviated, that is, $r_V = 1$. We define hysteresis as clockwise when sediment discharge peaks before water discharge. Undefined events correspond to both quantities peaking at the same time. Quantities are shown at distances 28.8, 29.4, and 30 km from the water input. The simulation is the same as that in Figure 6 (see also Table 4), but with dt = 900 s instead of dt = 3600 s to better resolve the hysteresis.

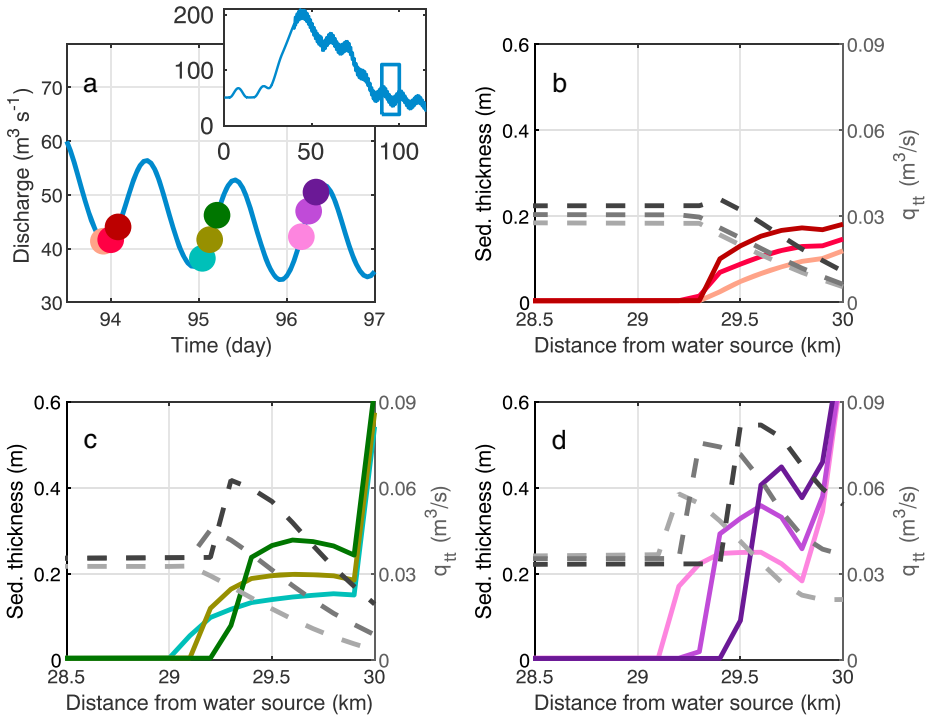

Figure 8. Example of snapshots of sediment deposits during a temporary sediment accumulation using the simulation shown in Figure 6 and 7. These snapshots are intended to represent the stratigraphy that could be observed in an esker deposit. (a) Water discharge at the terminus; the inset shows the entire season and the box shows the time plotted. The dots show the times at which panels (b–d) are displayed with matching colors. (b) Sediment thickness showing up-glacier accretion (km 29.4–30). (c) Sediment thickness showing vertical accretion (km 29.4–29.9) and scour (km 29–29.4). (d) Sediment thickness showing down-glacier accretion (km 29.6–29.8) and scour (km 29.1–29.6). In panels (b–d) increasing darkness of the colors represents increasing time during the simulation. The sediment discharge q_{tt} is plotted in dashed gray and increasing darkness represents increasing time.

hours. Note that a sediment-layer thickness less than the particle diameter ($\eta_a < D = 0.06$ m) does not preclude the presence of a sediment deposit, because non-uniform cross-channel sediment deposition is expected for bedrock channels (Chatanantavet & Parker, 2008; Nelson & Seminara, 2012).

During local minima in discharge, both the spatial and temporal bottlenecks occur simultaneously, sediment discharge gradient decreases monotonically toward the terminus, and sediment is deposited with an up-glacier accretionary pattern (Figure 8b); that is, sediment layers have a slope adverse to the direction of flow. As the discharge rises again, the upstream end of the deposited sediment wedge is advected down-flow while sediment discharge increases over the whole wedge. The sediment pulse in conjunction with the bottleneck produce an accretionary pattern between 29.4 and 29.9 km that is generally vertical (Figure 8c). When a large enough amount of sediment is deposited, the sediment pulse produces a sediment wave that travels toward the terminus and generates a down-glacier accretionary pattern between 29.6 and 29.8 km (Figure 8d).

To identify the main drivers of sediment deposition and thus of incipient esker deposition, we perform simulations where we vary independently: (1) ice surface profile, (2) water discharge, and (3) sediment input (Table 4). The steeper the ice-surface slope in the vicinity of the terminus, the sharper the sediment bottleneck, leading to relatively high but short sediment wedges (as high as 2.75 m but at most 300 m long for S2; Figures 9a–9d and Table 4). In a similar fashion, shallower ice-surface slopes yield a smoother bottleneck; therefore, sediment wedges tend to be longer but thinner (1.1 m high and at most 1.6 km long for S4). Changing the discharge by 20% has a limited effect on the extent of sediment deposition (1.4 km for S5 and 1.1 km for S6 for a decrease and increase in Q_{ch} by 20%, respectively; Table 4) although the thickness of sediment deposited increases with decreasing discharge (Figures 9e and 9f). Finally, the sediment input correlates well with the size of the temporary sediment wedge: The larger the sediment input, the larger the sediment wedge (Figures 9g and 9h).

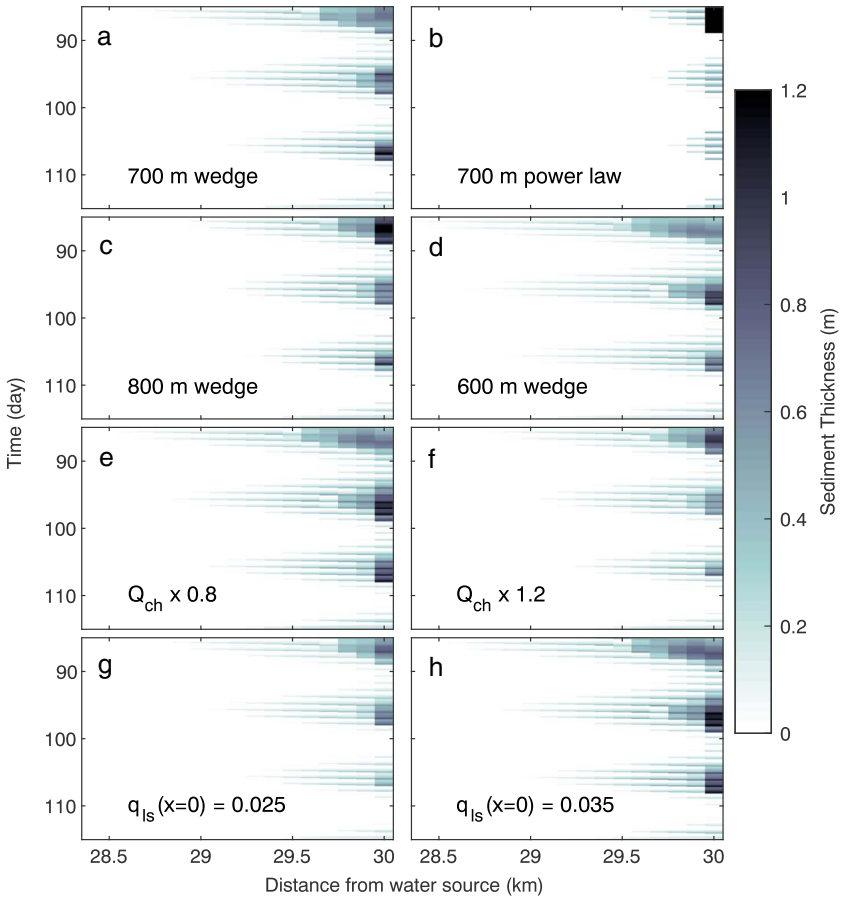

Figure 9. Evolution of sediment thickness (η_a) close to the terminus in the second part of the melt-season for the simulations described in Table 4. (a) Reference simulations shown in Figures 6, 7 and 8. (b)–(d) Effect of ice surface slope. (e)–(f) Effect of waster discharge. (g)–(h) Effect of sediment input.

4. Discussion

4.1. What Controls Sediment Delivery to Proglacial Streams?

Proglacial sediment yields have been widely used as a proxy for measuring contemporary erosion rates of glaciers (e.g., Bogen, 1996; Cowton et al., 2012; Hallet et al., 1996; Herman et al., 2015; Humphrey & Raymond, 1994; Koppes & Hallet, 2002; Koppes & Hallet, 2006; Koppes & Montgomery, 2009; Koppes et al., 2015; Loso et al., 2004; Riihimaki et al., 2005; Sanders et al., 2013). These studies are based on the assumption that subglacial sediment storage is minimal, such that sediment fluxes in the proglacial environment (stream, lake, and fjord) reflect erosion rates with little lag (e.g., Bogen, 1996; Cowton et al., 2012; Herman et al., 2015; Riihimaki et al., 2005). The common justifications for this assumption are that (1) the system is supply limited based on the hysteresis between sediment transport and water discharge (Herman et al., 2015; Mao et al., 2014; Riihimaki et al., 2005; Willis et al., 1996) or (2) an unrealistically thick layer of sediment would be required to sustain the measured sediment fluxes (e.g., Koppes & Hallet, 2002).

We suggest that hysteresis must be considered concurrently at different timescales (e.g., seasonal, multiday events of high- or low-melt, daily fluctuations) in order to produce a meaningful proxy for bed conditions. We show that even with our simple model setup and a supply-limited system over a whole season, bed conditions are expected to change rapidly. Typically, in a glacier system that is considered supply limited, sediment pulses have been attributed to (1) the removal of the sediment produced over the winter (e.g., Anderson et al., 1999; Cowton et al., 2012; Riihimaki et al., 2005), (2) enhanced basal water pressure related to an ice sliding event that can release sediment into a channel (e.g., Anderson et al., 2003; Willis et al., 1996), or (3) tapping into sediment pockets surrounding a channel by a subglacial flood (Anderson et al., 2003). In addition, we propose that temporary sediment deposition close to the terminus after significant drops in water input can create bed conditions conducive to subsequent sediment pulses. It is thus necessary to take into account

these four possible mechanisms, together with the hysteresis between sediment transport and water flow, to infer whether a glacier bed is supply or transport limited.

Sediment fluxes at the glacier terminus exhibit two distinct regimes during the modeled melt season, despite a constant sediment supply. The timing of the regime shift in outlet sediment flux is a function of the model setup ($q_{ls}(x = 0)$, $Q_{ch}(x = 0)$ magnitude and time-variance, ice geometry), yet this switch is expected for the majority of actively eroding glaciers. For example, we calculate that the range of sediment concentrations at the terminus for the second part of the melt season is 1–8 kg m^{-3} and is ~1.8 kg m^{-3} at the onset of alluviation. Published suspended sediment yields, which represent 30–70% of the total sediment flux, are on the order of 1–5 kg m^{-3} for a several-kilometer-long glacier in Alaska (Anderson et al., 1999; Riihimaki et al., 2005), 1–15 kg m^{-3} for a land-terminating outlet of the western Greenland Ice Sheet (Cowton et al., 2012), and 0.4–6.5 kg m^{-3} for Franz Joseph Glacier in the Southern Alps of New Zealand Herman et al. (2015). In these three cases, temporary sediment accumulation would be expected.

The sediment bottleneck in the vicinity of a glacier terminus is also likely to create a zone close to the margin where more sediment is present at the bed. In the current model, R-channels are assumed to remain pressurized; it is, however, common for land-terminating glacier termini to display an ice-roofed river flowing at atmospheric pressure. The transport capacity of such a river is expected to be less than that of a pressurized R-channel, and sediment is therefore likely to accumulate. An actively eroding glacier with a dominantly supply-limited bed could still therefore produce sediment yields with behavior tied to a subglacial alluvial channel.

Recent studies have shown that the total contribution of the Greenland Ice Sheet system to subglacial sediment (Overeem et al., 2017) and nutrient fluxes (Bhatia et al., 2013) represents a significant fraction of global budgets. Understanding how these fluxes will evolve in a changing climate is thus key to projecting the response of ecosystems in affected areas. Both studies postulate that these fluxes should increase with increasing melt-water production. As temperatures rise, water discharge will increase; however, the ice thins faster than it retreats, producing a tendency for ice-surface slopes to decrease. Based on our simulations (Figure 9), low ice-surface slopes promote sediment deposition, thereby hindering sediment delivery to the ocean from land-terminating glaciers. Further from the terminus, the channel bed is expected to be supply limited, thus increasing the sediment or nutrient fluxes requires enhanced production and glacial erosion rates.

4.2. What Controls Sediment Deposition and Formation of Incipient Eskers?

Previous works on eskers have addressed the spatial controls on their location and implications for water and sediment supply (e.g., Brennand, 1994, 2000; Burke et al., 2012; Burke et al., 2015; Clark & Walder, 1994; Knight, 2003; Storrar et al., 2014). It is, however, rare to find a process-based explanation as to why the subglacial channelized water flow should deposit sediment. Esker sediments are recognized to originate from highly dynamic water flows or changes in cross-sectional area along the flow path, and subglacial floods are invoked to explain the presence of cobbles and boulders (e.g., Brennand, 1994, 2000; Burke et al., 2012, 2015; Clark & Walder, 1994). Using a simple theory of subglacial water flow along hydraulic potential gradients (Shreve, 1972) would indicate that water flow speed increases toward the terminus as the slope of the ice steepens (e.g., Alley et al., 1997; Clark & Walder, 1994), promoting sediment evacuation rather than deposition.

The results presented here provide a mechanism for sediment deposition near a glacier terminus: a spatio-temporal bottleneck in sediment transport inherent to the dynamics of water flow in subglacial channels and thinning ice toward the terminus. In the presence of a sufficient sediment supply, this bottleneck leads to sediment deposition in the vicinity of the terminus, which can be interpreted as an incipient esker. The waning of water discharge in a forcing cycle (synthetic melt season) is particularly conducive to sediment deposition. Discharge fluctuations over the course of ~1–4 weeks (Figures 4 to 6) results in the largest sediment volumes deposited. On these timescales, discharge can decrease faster than creep can close the channel walls to sustain hydraulic pressure gradients but leaves a significant amount of time for sediment to accumulate. With water input fluctuations of a period less than a week, the window for sediment deposition is limited by the increase in discharge that tends to flush the sediment. When input discharge decreases over longer periods of time, the constriction of the channel by creep is large enough that hydraulic potential gradients only drop slightly, inhibiting the bottleneck effect.

Our results suggest that ice-surface slope and the pattern of water input to the channel are perhaps as important, if not more, than sediment availability and the total amount of meltwater production. This is particularly

evident in the simulation where the ice surface follows a power-law profile (see S2 in Table 4 and Figure S5); this simulation produced the least sediment deposition even though the ice-surface slope at the terminus is only 7.5%. This strongly reinforces the idea that ice sheets deposit eskers during retreat (e.g., Brennand, 1994, 2000; Burke et al., 2015; Storrar et al., 2014), when ice-surface slopes are shallow due to the melting and thinning.

The modeled dynamics of the sediment-bearing R-channel fed by fluctuating water input produced simulated sedimentary deposits (Figure 8) that closely match those observed in esker ridges in southern Alberta (Burke et al., 2015). In our simulations the sediment pulses occur because of temporary sediment accumulation, although the mechanisms that could produce sediment pulses discussed in the previous section would also lead to these deposits. Changes in glacier geometry will affect the hydraulic potential gradient, and the presence of bed slopes adverse to ice and water flow (Werder, 2016) would also result in a sediment bottleneck. Sediment on bed slopes adverse to the direction of flow can be transported by basal freeze-on (Creyts et al., 2013) and is more likely to be deformed by ice flow.

In this study we have not explicitly addressed the issue of different particle diameters. However, we calculate that if we had used $D = 0.005$ m, instead of $D = 0.06$ m, temporary sediment deposition would still occur with a sediment input rate as low as $q_{ls} = 0.015\ m^3\ s^{-1}$, half of what we prescribe. Since the sediment input rates we impose are conservative compared to values estimated in the field (see previous section), our results should hold true across a wide range of parameters. Finally, we model maximum bed shear stress values of 450–780 Pa over the last 10 km of the glacier profiles, indicating that meter-sized boulders could readily be mobilized by seasonal water flow (Beaud et al., 2016, 2018).

5. Conclusions

We present the first one-dimensional framework for morphodynamics in sediment-bearing R-channels, by combining water and sediment flow for mixed alluvial-bedrock conditions. We show that channelized water flow under a land-terminating glacier inherently creates a bottleneck in sediment transport near the terminus. In the presence of a sufficient sediment supply, this bottleneck leads to an accumulation of sediment near the terminus, whereas the rest of the channel experiences supply-limited conditions. The bottleneck is accentuated by temporal fluctuations in water discharge, in particular when these fluctuations have periods greater than several days and up to several weeks. Interestingly, the coupling with sediment transport has a significant impact on sediment deposition, omitting this feedback in numerical models would lead to overestimated sediment deposition and underestimated sediment fluxes.

The waning phase of a melt season is particularly prone to temporary sediment accumulation and deposition of an incipient esker. This temporary alluviation of the R-channel bed can drive proglacial sediment fluxes and, as a result, challenge our current interpretation of hysteresis between sediment and water discharge. We recommend a reanalysis of such hysteresis across a range of timescales throughout the melt-season in order to avoid the bias of specific events. We also recommend examining proxies that would indicate possible sources of sediment pulses during these hysteresis cycles.

We propose that esker deposition is a natural feature of channelized water flow under land-terminating glaciers. Provided that the sediment supply is sufficient, we expect that an esker would, at least temporarily, be deposited at the end of a melt season. The fate of such an esker would be determined by the subsequent state of the subglacial environment near the terminus. For example, a retreating ice sheet would exhibit a thinning terminus, favorable for further sediment deposition and the growth of an esker. On the other hand, an advancing ice sheet would exhibit a steepened terminus resulting in higher shear stresses favorable for flushing previously stored sediment. Our results support time-transgressive deposition of eskers by retreating ice sheets and suggest that sudden deposition of esker segments longer than a few kilometers is unlikely.

Notation

$\tilde{A}$ flow-law coefficient for channels ($5 \times 10^{-25}\ Pa^{-n}\ s^{-1}$)
$\dot{b}_{ch}$ local water input to the channel ($m^2\ s^{-1}$)
c_t pressure melting coefficient ($K\ Pa^{-1}$)
c_w heat capacity of water ($J\ kg^{-1}\ K^{-1}$)

D	particle diameter (m)
dt	time step (s)
dx	grid cell size (m)
f_b	Darcy-Weisbach roughness of the bed
f_i	Darcy-Weisbach roughness of the ice
f_R	channel-averaged Darcy-Weisbach roughness
F_c	fraction of covered bedrock
g	gravitational acceleration (9.8 m s^{-2})
h_i	ice thickness (m)
L	latent heat of fusion (J kg^{-1})
n	exponent of Glen's flow law
n'_i	Manning roughness of ice
n'_b	Manning roughness of the bed
$\langle n' \rangle$	channel-averaged Manning roughness
N_{ch}	effective pressure in the channel (Pa)
p_{ch}	water pressure in the channel (Pa)
p_i	ice overburden pressure (Pa)
P_b	bed perimeter of channel (m)
P_i	ice perimeter of channel (m)
P_W	wetted perimeter of channel (m)
q_{ls}	local source of volumetric sediment flux per unit width (m^3 s^{-1})
q_t	volumetric rate of sediment transport per unit width (m^2 s^{-1})
q_{tt}	volumetric rate of sediment transport (m^3 s^{-1})
q_{tc}	volumetric transport capacity per unit width (m^2 s^{-1})
q_{ttc}	volumetric transport capacity (m^3 s^{-1})
Q_{ch}	water discharge (m^3 s^{-1})
r	buoyant density of submerged particle
R_H	hydraulic radius of channel (m)
r_V	ratio between available sediment volume and volume at transport capacity
S_{ch}	channel cross-sectional area (m^2)
v	water velocity in channel (m s^{-1})
u_s	depth-averaged streamwise bed load velocity (m s^{-1})
v_{oc}	channel opening rate by viscous heat dissipation (m^2 s^{-1})
v_{cc}	channel creep closure rate (m^2 s^{-1})
v_s	channel closure rate by sediment deposition (m^2 s^{-1})
V_s	volume of sediment per unit length (m^2)
V_b	volume of transient sediment per unit width and length (m)
V_{bal}	balance between sediment input and output fluxes per time step (m^3)
V_{tc}	volume of sediment per unit width and length at saturation for transport (m^2)
W_{ch}	channel width (m)
X_L	glacier length (m)
z_b	elevation of bed surface (alluvium and bedrock) (m)
z_i	elevation of glacier surface (m)
λ	porosity of bed sediment
γ	fluid compressibility factor (Pa^{-1})
η_a	Thickness of sediment above bedrock (m)
η_{br}	elevation of bedrock surface (m)
ρ_i	ice density (kg m^{-3})
ρ_s	particle density (kg m^{-3})
ρ_w	water density (kg m^{-3})
Π	sensible heat change of water (W m^{-1})
τ_b	basal shear stress (Pa)
τ_{tot}	total shear stress at the flow boundary (Pa)
τ^*	nondimensional boundary shear stress

τ_c^* threshold nondimensional boundary shear stress for particle motion
ϕ_{ch} hydraulic potential in the channel (Pa)
Ξ dissipation of potential energy (W m^{-1})

Acknowledgments
We would like thank the editor in chief, Bryn Hubbard, as well as two anonymous reviewers for their constructive comments on the manuscript. Funding was provided by the Swiss National Cooperative for the Disposal of Radioactive Waste (Nagra) within the framework of investigating ice-age effects related to the long-term safety of radioactive waste disposal. Funding was also provided by the Natural Sciences and Engineering Research Council of Canada (NSERC), the Canada Research Chairs Program, and Simon Fraser University (SFU). F. Beaud would like to acknowledge funding from the Swiss National Science Fund through an Early-Mobility postdoctoral fellowship. The simulations used for the paper can be downloaded here: https://researchdata.sfu.ca/pydio_public/beaud_etal_jgr_simulation_repo. The code can be dowloaded from the following repository: https://bitbucket.org/Flavien/beaud_etal_jgr_code_r-channel/src/master/. The authors declare no conflict of interest.

References

Alley, R. B., Cuffey, K. M., Evenson, E. B., Strasser, J. C., Lawson, D. E., & Larson, G. J. (1997). How glaciers entrain and transport basal sediment: Physical constraints. *Quaternary Science Reviews*, *16*(9), 1017–1038.

Anderson, S. P., Fernald, K. M., Anderson, R. S., & Humphrey, N. F. (1999). Physical and chemical characterization of a spring flood event, bench glacier, alaska, USA: Evidence for water storage. *Journal of Glaciology*, *45*(150), 177–189.

Anderson, S. P., Walder, J. S., Anderson, R. S., Kraal, E. R., Cunico, M., Fountain, A. G., & Trabant, D. C. (2003). Integrated hydrologic and hydrochemical observations of hidden creek lake Jökulhlaups, Kennicott Glacier, Alaska. *Journal of Geophysical Research*, *108*(F1), 6003. https://doi.org/10.1029/2002JF000004

Beaud, F., Flowers, G. E., & Venditti, J. G. (2016). Efficacy of bedrock erosion by subglacial water flow. *Earth Surface Dynamics*, *4*, 125–145. https://doi.org/doi:10.5194/esurf-4-125-2016

Beaud, F., Venditti, J. G., Flowers, G. E., & Koppes, M. (2018). Excavation of subglacial bedrock channels by seasonal meltwater flow. *Earth Surface Processes and Landforms*, *43*(9), 1960–1972. https://doi.org/10.1002/esp.4367

Bennett, M. R., & Glasser, N. F. (2009). *Glacial geology: Ice sheets and landforms* (2nd ed.). The Atrium, Chichester, West Sussex, UK: John Wiley & Sons Ltd.

Bhatia, M. P., Kujawinski, E. B., Das, S. B., Breier, C. F., Henderson, P. B., & Charette, M. A. (2013). Greenland meltwater as a significant and potentially bioavailable source of iron to the ocean. *Nature Geoscience*, *6*(4), 274.

Bogen, J. (1996). Erosion rates and sediment yields of glaciers. *Annals of Glaciology*, *22*(1), 48–52.

Brennand, T. A. (1994). Macroforms, large bedforms and rhythmic sedimentary sequences in subglacial eskers, south-central ontario: Implications for esker genesis and meltwater regime. *Sedimentary Geology*, *91*(1), 9–55.

Brennand, T. A. (2000). Deglacial meltwater drainage and glaciodynamics: Inferences from Laurentide eskers, Canada. *Geomorphology*, *32*(3), 263–293.

Burke, M. J., Brennand, T. A., & Perkins, A. J. (2012). Transient subglacial hydrology of a thin ice sheet: Insights from the chasm esker, british Columbia, Canada. *Quaternary Science Reviews*, *58*, 30–55.

Burke, M. J., Brennand, T. A., & Sjogren, D. B. (2015). The role of sediment supply in esker formation and ice tunnel evolution. *Quaternary Science Reviews*, *115*, 50–77.

Carter, S. P., Fricker, H. A., & Siegfried, M. R. (2017). Antarctic subglacial lakes drain through sediment-floored canals: Theory and model testing on real and idealized domains. *The Cryosphere*, *11*(1), 381.

Chatanantavet, P., & Parker, G. (2008). Experimental study of bedrock channel alluviation under varied sediment supply and hydraulic conditions. *Water Resources Research*, *44*, W12446. https://doi.org/10.1029/2007WR006581

Church, M., & Ryder, J. M. (1972). Paraglacial sedimentation: A consideration of fluvial processes conditioned by glaciation. *Geological Society of America Bulletin*, *83*(10), 3059–3072.

Clark, P. U., & Walder, J. S. (1994). Subglacial drainage, eskers, and deforming beds beneath the Laurentide and Eurasian ice sheets. *Geological Society of America Bulletin*, *106*(2), 304–314.

Clarke, G. K. C. (2003). Hydraulics of subglacial outburst floods: New insights from the Spring-Hutter formulation. *Journal of Glaciology*, *49*(165), 299–313.

Cowton, T., Nienow, P., Bartholomew, I., Sole, A., & Mair, D. (2012). Rapid erosion beneath the Greenland ice sheet. *Geology*, *40*(4), 343–346.

Creyts, T. T., Clarke, G. K. C., & Church, M. (2013). Evolution of subglacial overdeepenings in response to sediment redistribution and glaciohydraulic supercooling. *Journal of Geophysical Research: Earth Surface*, *118*, 423–446. https://doi.org/10.1002/jgrf.20033

Damsgaard, A., Suckale, J., Piotrowski, J. A., Houssais, M., Siegfried, M. R., & Fricker, H. A. (2017). Sediment behavior controls equilibrium width of subglacial channels. *Journal of Glaciology*, *63*(242), 1034–1048.

Delaney, I., Bauder, A., Huss, M., & Weidmann, Y. (2018). Proglacial erosion rates and processes in a glacierized catchment in the Swiss Alps. *Earth Surface Processes and Landforms*, *43*(4), 765–778.

Denton, G. H., & Sugden, D. E. (2005). Meltwater features that suggest miocene ice-sheet overriding of the transantarctic mountains in Victoria Land, Antarctica. *Geografiska Annaler: Series A, Physical Geography*, *87*, 67–85.

Drews, R., Pattyn, F., Hewitt, I., Ng, F., Berger, S., Matsuoka, K., et al. (2017). Actively evolving subglacial conduits and eskers initiate ice shelf channels at an antarctic grounding line. *Nature Communications*, *8*(15), 228.

Dürst-Stucki, M., Reber, R., & Schlunegger, F. (2010). Subglacial tunnel valleys in the alpine foreland: An example from Bern, Switzerland. *Swiss Journal of Geosciences*, *103*(3), 363–374.

Dürst-Stucki, M., Schlunegger, F., Christener, F., Otto, J.-C., & Götz, J. (2012). Deepening of inner gorges through subglacial meltwater—An example from the UNESCO Entlebuch Area, Switzerland. *Geomorphology*, *139*, 506–517.

Einstein, H. A. (1950). The bed-load function for sediment transportation in open channel flows (Vol. *1026*). Washington, DC: US Department of Agriculture, Soil Conservation Service.

Fernandez-Luque, R., & van Beek, R. (1976). Erosion and transport of bed-load sediment. *Journal of Hydraulic Research*, *14*(2), 127–144.

Fischer, U. H., Bebiolka, A., Brandefelt, J., Follin, S., Hirschorn, S., Jensen, M., et al. (2015). Chapter 11: Radioactive waste under conditions of future ice ages. In W. Haeberli & Hazard and Disasters Series (Eds.), *Snow and ice-related hazards, risks, and disasters* (pp. 345–393). Academic Press Waltham, MA: Elsevier.

Flowers, G. E. (2015). Modelling water flow under glaciers and ice sheets. *Proceedings of the Royal Society of London A: Mathematical, Physical and Engineering Science*, *471*(2176), 1–41. https://doi.org/10.1098/rspa.2014.0907

Flowers, G. E., Björnsson, H., Pálsson, F., & Clarke, G. K. C. (2004). A coupled sheet-conduit mechanism for Jökulhlaup propagation. *Geophysical Research Letters*, *31*, L05401. https://doi.org/10.1029/2003GL019088

Fowler, A., & Walder, J. (1993). Creep closure of channels in deforming subglacial till. *Proceedings of the Royal Society of London A: Mathematical, Physical and Engineering Science*, *441*, 17–31.

Garcia, M. H. (2000). The legend of A.F. shields. *Journal of Hydraulic Engineering*, *126*(9), 718–720.

García, M. H. (2008). *Sedimentation Engineering: Processes, Measurements, Modeling, and Practice* (Vol. 110). Reston, VA: ASCE Publications.

Greenwood, S. L., Clason, C. C., Helanow, C., & Margold, M. (2016). Theoretical, contemporary observational and palaeo-perspectives on ice sheet hydrology: Processes and products. *Earth-Science Reviews*, *155*, 1–27.

Gulley, J. D., Spellman, P. D., Covington, M., Martin, J. B., Benn, D. I., & Catania, G. (2014). Large values of hydraulic roughness in subglacial conduits during conduit enlargement: Implications for modeling conduit evolution. *Earth Surface Processes and Landforms*, *39*(3), 296–310.

Gurnell, A. M., Hannah, D., & Lawler, D. (1996). Suspended sediment yield from glacier basins. *IAHS Publications-Series of Proceedings and Reports-Intern Assoc Hydrological Sciences*, *236*, 97–104.

Hallet, B., Hunter, L., & Bogen, J. (1996). Rates of erosion and sediment evacuation by glaciers: A review of field data and their implications. *Global and Planetary Change*, *12*(1-4), 213–235.

Herman, F., Beyssac, O., Brughelli, M., Lane, S. N., Leprince, S., Adatte, T., et al. (2015). Erosion by an alpine glacier. *Science*, *350*(6257), 193–195.

Humphrey, N. F., & Raymond, C. F. (1994). Hydrology, erosion and sediment production in a surging glacier: Variegated Glacier, Alaska, 1982-83. *Journal of Glaciology*, *40*(136), 539–552.

Inoue, T., Izumi, N., Shimizu, Y., & Parker, G. (2014). Interaction among alluvial cover, bed roughness, and incision rate in purely bedrock and alluvial-bedrock channel. *Journal of Geophysical Research: Earth Surface*, *119*, 2123–2146. https://doi.org/10.1002/2014JF003133

Jansen, J. D., Codilean, A. T., Stroeven, A. P., Fabel, D., Hättestrand, C., Kleman, J., et al. (2014). Inner gorges cut by subglacial meltwater during Fennoscandian ice sheet decay. *Nature Communications*, *5*, 3815. https://doi.org/10.1038/ncomms4815

Jørgensen, F., & Sandersen, P. B. E. (2006). Buried and open tunnel valleys in Denmark—Erosion beneath multiple ice sheets. *Quaternary Science Reviews*, *25*(11), 1339–1363.

Kehew, A. E., Piotrowski, J. A., & Jørgensen, F. (2012). Tunnel valleys: Concepts and controversies—A review. *Earth-Science Reviews*, *113*(1), 33–58.

Knight, J. (2003). Bedform patterns, subglacial meltwater events, and Late Devensian ice sheet dynamics in north-central Ireland. *Global and Planetary Change*, *35*(3), 237–253.

Koppes, M. N., & Hallet, B. (2002). Influence of rapid glacial retreat on the rate of erosion by tidewater glaciers. *Geology*, *30*(1), 47–50.

Koppes, M., & Hallet, B. (2006). Erosion rates during rapid deglaciation in Icy Bay, Alaska. *Journal of Geophysical Research*, *111*, F02023. https://doi.org/10.1029/2005JF000349

Koppes, M., Hallet, B., Rignot, E., Mouginot, J., Wellner, J. S., & Boldt, K. (2015). Observed latitudinal variations in erosion as a function of glacier dynamics. *Nature*, *526*(7571), 100–103.

Koppes, M. N., & Montgomery, D. R. (2009). The relative efficacy of fluvial and glacial erosion over modern to orogenic timescales. *Nature Geoscience*, *2*(9), 644–647.

Kyrke-Smith, T. M., & Fowler, A. C. (2014). Subglacial swamps. *Proceedings of the Royal Society of London A: Mathematical, Physical and Engineering Science*, *470*(2171), 20140340.

Lamb, M. P., Dietrich, W. E., & Sklar, L. S. (2008). A model for fluvial bedrock incision by impacting suspended and bed load sediment. *Journal of Geophysical Research*, *113*, F03025. https://doi.org/10.1029/2007JF000915

Lamb, M. P., Dietrich, W. E., & Venditti, J. G. (2008). Is the critical shields stress for incipient sediment motion dependent on channel-bed slope? *Journal of Geophysical Research (2003–2012)*, *113*, F02008. https://doi.org/10.1029/2007JF000831

Livingstone, S. J., & Clark, C. D. (2016). Morphological properties of tunnel valleys of the southern sector of the Laurentide Ice Sheet and implications for their formation. *Earth Surface Dynamics*, *4*(3), 567.

Loso, M. G., Anderson, R. S., & Anderson, S. P. (2004). Post-Little Ice Age record of coarse and fine clastic sedimentation in an Alaskan proglacial lake. *Geology*, *32*(12), 1065–1068.

Mao, L., Dell'Agnese, A., Huincache, C., Penna, D., Engel, M., Niedrist, G., & Comiti, F. (2014). Bedload hysteresis in a glacier-fed mountain river. *Earth Surface Processes and Landforms*, *39*(7), 964–976.

Meyer-Peter, E., & Müller, R. (1948). Formulas for bed-load transport. In *Proceedings of the 2nd meeting of the international association for hydraulic structures research* (pp. 39–64). Stockholm: IAHR.

Nelson, P. A., & Seminara, G. (2012). A theoretical framework for the morphodynamics of bedrock channels. *Geophysical Research Letters*, *39*, L06408. https://doi.org/10.1029/2011GL050806

Ng, F. S. L. (2000). Canals under sediment-based ice sheets. *Annals of Glaciology*, *30*(1), 146–152.

Nye, J. F. (1976). Water flow in glaciers: Jökulhlaups, tunnels and veins. *Journal of Glaciology*, *17*, 181–207.

Ó Cofaigh, C. (1996). Tunnel valley genesis. *Progress in Physical Geography*, *20*(1), 1–19.

Orwin, J. F., & Smart, C. C. (2004). Short-term spatial and temporal patterns of suspended sediment transfer in proglacial channels, small river glacier, Canada. *Hydrological Processes*, *18*(9), 1521–1542.

Overeem, I., Hudson, B. D., Syvitski, J. P., Mikkelsen, A. B., Hasholt, B., van den Broeke, M., et al. (2017). Substantial export of suspended sediment to the global oceans from glacial erosion in Greenland. *Nature Geoscience*, *10*(11), ngeo3046.

Riihimaki, C. A., MacGregor, K. R., Anderson, R. S., Anderson, S. P., & Loso, M. G. (2005). Sediment evacuation and glacial erosion rates at a small alpine glacier. *Journal of Geophysical Research*, *110*, F03003. https://doi.org/10.1029/2004JF000189

Röthlisberger, H. (1972). Water pressure in intra- and subglacial channels. *Journal of Glaciology*, *11*(62), 177–203.

Sanders, J. W., Cuffey, K. M., MacGregor, K. R., & Collins, B. D. (2013). The sediment budget of an alpine cirque. *Geological Society of America Bulletin*, *125*(1-2), 229–248.

Shields, A. (1936). Anwendung der Aehnlichkeitsmechanik und der Turbulenzforschung auf die Geschiebebewegung (PhD thesis Technical University Berlin), Mitteilungen der Preussichen Versuchsanstalt für Wasserbau und Schiffbau, Berlin. Retrieved from Delft University of Technology database (digital copy 2005).

Shreve, R. L. (1972). Movement of water in glaciers. *Journal of Glaciology*, *11*, 205–214.

Sklar, L. S., & Dietrich, W. E. (2004). A mechanistic model for river incision into bedrock by saltating bed load. *Water Resources Research*, *40*, W06301. https://doi.org/10.1029/2003WR002496

Storrar, R. D., Stokes, C. R., & Evans, D. J. A. (2014). Increased channelization of subglacial drainage during deglaciation of the Laurentide Ice Sheet. *Geology*, *42*(3), 239–242.

Stumm, D. (2010). Deep glacial erosion. Review with focus on tunnel valleys in northern Europe (NAB 10-33): National Genossenschaft für die Lagerung radioaktiver Abfälle, Wettingen, Switzerland.

van der Vegt, P., Janszen, A., & Moscariello, A. (2012). Tunnel valleys: Current knowledge and future perspectives. *Geological Society, London, Special Publications*, *368*(1), 75–97.

Walder, J. S., & Fowler, A. (1994). Channelized subglacial drainage over a deformable bed. *Journal of Glaciology*, *40*, 3–15.

Werder, M. A. (2016). The hydrology of subglacial overdeepenings: A new supercooling threshold formula. *Geophysical Research Letters*, *43*, 2045–2052. https://doi.org/10.1002/2015GL067542

Werder, M. A., Hewitt, I. J., Schoof, C., & Flowers, G. E. (2013). Modeling channelized and distributed drainage in two dimensions. *Journal of Geophysical Research: Earth Surface*, *118*, 2140–2158. https://doi.org/10.1002/jgrf.20146

Willis, I. C., Richards, K. S., & Sharp, M. J. (1996). Links between proglacial stream suspended sediment dynamics, glacier hydrology and glacier motion at Midtdalsbreen, Norway. *Hydrological Processes*, *10*(4), 629–648.

Wright, H. E. (1973). Tunnel valleys, glacial surges, and subglacial hydrology of the Superior Lobe, Minnesota. *Geological Society of America Memoirs*, *136*, 251–276.

Zhang, L., Parker, G., Stark, C. P., Inoue, T., Viparelli, E., Fu, X., & Izumi, N. (2015). Macro-roughness model of bedrock-alluvial river morphodynamics. *Earth Surface Dynamics*, *3*(1), 113–138.